Utrecht University

Bachelor Thesis

Optimisation of the B^0 reconstruction in Pb-Pb collisions at $\sqrt{s_{NN}} = 5.5$ TeV using the upgraded ALICE detector

Author:
Maarten van de Pas
Utrecht University

Daily Supervisor:
Dr. Alessandro Grelli
Utrecht University

Supervisor:
Dr. Andre Mischke
Utrecht University

At the
Faculty of Sciences
Institute for Subatomic Physics

June 2015

Abstract

The Quark Gluon Plasma (QGP) is a state of matter predicted by Quantum Chromodynamics. At sufficiently high temperatures and (energy) densities, QCD predicts that the constituent particles of hadronic matter are no longer confined to their hadrons and behave as asymptotically free particles within the plasma.Since 2010, CERN's Large Hadron Collider, near Geneva, has been producing this state of matter by colliding highly energetic, dense atomic nuclei and observing the resulting 'debris'.

In this thesis, we study the reconstruction of the B^0 meson through its hadronic decay channel, produced in lead-lead colissions with center of mass energies of $\sqrt{s_{NN}} = 5.5$ TeV, in the upgraded ALICE detector as is planned to be implemented during the LHC's second long shutdown. We focus on the improvements that can be made on cuts of the D^{*+} invariant mass in transverse momentum intervals [1,3], [3, 5], [5, 8], [8, 16] and [16, 24] GeV/c, with respect to the current detector and explore additional cuts to improve the B^0 invariant mass signal.

Unfortunately, the cuts laid out in this thesis do not improve the statistical significance enough to reach observation levels. Further studies of cuts are required.

Contents

1 Introduction

In this thesis we study the reconstruction of B^0 mesons in $\sqrt{s_{NN}} = 5.5$ TeV Pb-Pb collisions in the upgraded ALICE detector as planned for LHC Run-3 (scheduled to start in 2020 [1]). In order to implement cuts on the combinatorial background in these collisions, we compare the accuracies of the reconstructed D^{*+} meson invariant mass in the upgraded ALICE detector and the non-upgraded detector. Furthermore, we investigate the effects on the background and signal of the B^0 invariant mass, by cutting on the D^{*+} invariant mass, as well as by implementing additional topological cuts.

1.1 The Standard Model

Particle physics, which concerns itself with the study of the elementary building blocks of our world, has made enormous strides in improving our understanding of the world around us. In little over a century the boundaries of our understanding of the world of particle physics have leaped from atoms to nuclei and electrons, from nuclei to protons and neutrons and eventually to the particles that make up the Standard Model. With each step came new quantum (field) theories which came to describe the electromagnetic, weak and strong interactions.

The Standard Model, since it's finalization in the 1970's, is a unification of the quantum field theories of the Electroweak and Strong nuclear interactions and their elementary particles. As such the Standard model describes 12 fermionic particles, which constitute matter, 4 gauge bosons which mediate the three forces between the particles of matter, as well as the (recently discovered) Higgs Boson [2].

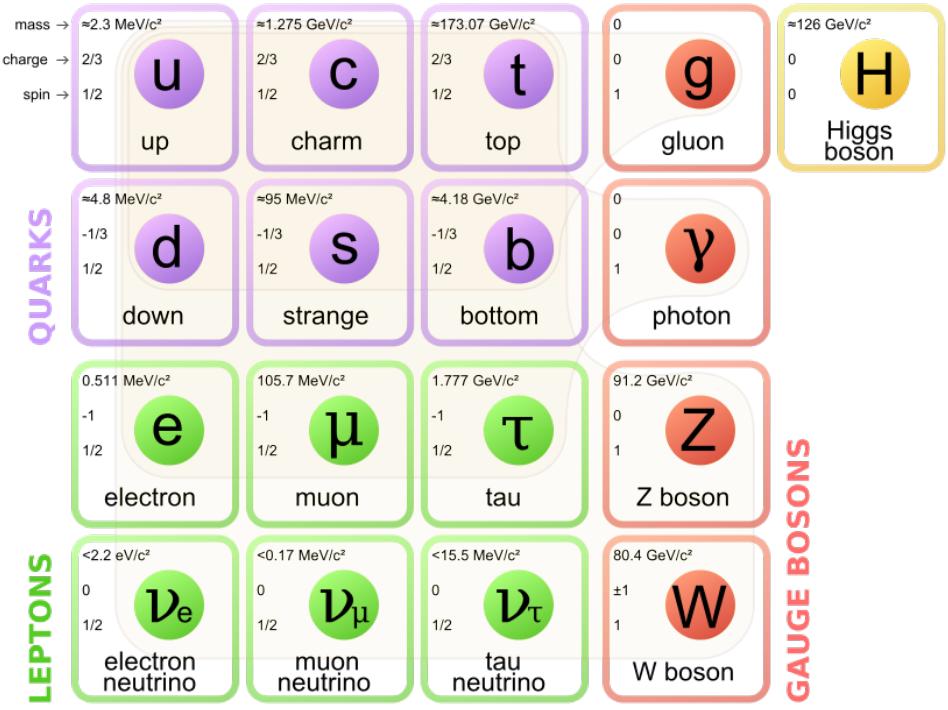

Figure 1: The particles of the Standard Model [3].

The fermionic particles consist of two groups, both consisting of three generations of particles. One group contains the leptons: the electron, muon, tauon and their respective (un-

charged) neutrinos. The other contains the quarks, in order of ascending mass: up, down, strange, charm, bottom and top. Note that the bottom quark is also known as beauty, and shall be referred to as such in this thesis. Of these two groups, only the quarks take part in strong interactions via Quantum Chromodynamics.

The gauge bosons each correspond to one type of interaction. Photons are the mediators of electromagnetic charge, whilst the $W^{\pm}$ and Z bosons mediate the weak nuclear force. Of particular interest for this thesis are the gluons which mediate the strong nuclear force.

Despite the experimental successes of the Standard Model, which include the discovery of the Higgs boson, it is not a full theory of the universe as it does not include the final fundamental interaction: gravity.

1.2 Quantum Chromodynamics and the Quark Gluon Plasma

Quantum Chromodynamics (QCD) is a Quantum Field Theory which describes the workings of the strong nuclear force, which acts not only upon quarks but also upon its own force mediators, the gluons. Like how Quantum Electrodynamics describes the mediation of electrodynamics by photons coupled to the electric charge, QCD gluons couple to a so called 'colour' charge. Each quark has a colour charge (r, g, b) while anti-colour states $(\bar{r}, \bar{g}, \bar{b})$ are available only to anti-quarks [4].

Whereas (anti)quarks only carry a single colour charge, gluons carry a colour and anti-colour. This gives rise to 9 possible gluon colour states. However, since there are no long range gluon interactions between colourless baryons, the colour(less) state $(r\bar{r}+b\bar{b}+g\bar{g})/\sqrt{3}$ cannot exist.

Since gluons carry colours, they are self interacting. Though at small distances the potential behaves much like that of QED, at longer distances the interactions between the gluons will cause the field strength to remain constant over distance, yielding a QCD potential of the form

$$V_{QCD}(r) = -\frac{4}{3}\frac{\alpha_s}{r} + \lambda r, \tag{1}$$

where α_s is the strong coupling constant, which has the following proportionality

$$\alpha_s(Q^2) \propto 1/\ln\frac{Q^2}{\Lambda^2_{QCD}}. \tag{2}$$

This string like potential term leads to a phenomenon called confinement, gluons and quarks are confined to hadrons and cannot be observed as free particles.

However, the coupling constant has an explicit dependence on the four-momentum transfer Q. As Q becomes bigger, the coupling constant becomes smaller. For sufficiently small distances and energies (which correspond to large Q^2), it is hypthosized that the coupling becomes neglible and quarks and gluons behave as freely interacting particles (see Fig. 2. Quarks and gluons in this state form the Quark Gluon Plasma (QGP).

It is thought that the conditions of the early universe (up to a few μs after the Big Bang), caused matter to exist as a QGP, via the means of very high pressures and temperature. The QGP is also exactly what heavy ion colliders, such as the LHC and RHIC, aim to produce by colliding highly energetic heavy ions in order to create high local temperatures and densities.

QGPs created in heavy ion collisions are too short-lived in order to observe directly. Once the QGP expands sufficiently, the coupling constant becomes high enough that the gluons and quarks hadronize into mesons and baryons. This phase transition from the QGP into final state hadronic particles occurs at the femtometer scale. This leaves only indirect measurements of the QGP via the produced hadrons.

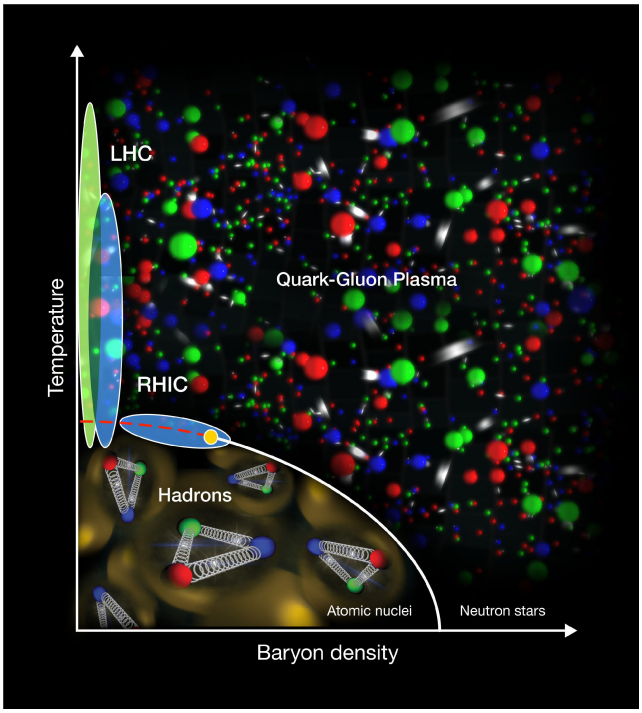

Figure 2: Phase diagram of hadronic matter to QGP. The pressure and temperature ranges attainable by RHIC [5] and the LHC are marked.

1.3 Heavy Flavour as a probe of the QGP

As partons of the incoming hadrons collide with energies $\geq 2m_q$, they may produce heavy flavour quark pairs. This may happen when a gluon annihilates with another gluon, giving rise to a quark and antiquark pair. Similarly, a quark and anti-quark may annihilate to form a heavier quark, anti-quark pair. The production time of quarks scales with $1/m_q$ where m_q is the quark mass. As such, charm, beauty and top form before the QGP itself [6], and can interact with the medium. However, due to the high mass of the top, it decays via electroweak interactions before it can hadronize.

As particles pass through the medium, they will lose energy to the QGP via means of gluon bremsstrahlung. Heavy flavour quarks however, are subjected to the so called 'dead-cone' effect [7]. This states that for gluon radiation angles $\theta \leq m_q/E$, the energy loss via the gluon bremsstrahlung is suppressed significantly when compared to light quarks. This reduces the chances that the heavy quarks lose too much energy through gluon radiation and becomes absorbed in the QGP. Conversely, the chances that these heavy quarks hadronise into mesons which we can reconstruct, increases.

Since the heavy quarks can be created regardless of nucleon density, we can compare the transverse momentum distributions of heavy quark (mesons) produced in p-p collisions with those of heavy quarks produced in Pb-Pb collisions. This yields the nuclear modification

factor R_{AA}

$$R_{AA} = \frac{1}{\langle T_{AA} \rangle} \frac{d^2 N_{AA}/d\eta dp_T}{d\sigma_{pp} dp_T}, \tag{3}$$

where T_{AA} is the normalization factor, accounting for the fact that lead has 207 nucleons taking part in the collision, whereas the proton only has one. In the case that there is no (interacting) QGP, we expect the R_{AA} to be equal to one. After all, the heavy quarks form in the same way for both events and in neither case do the quarks lose energy to a (QGP) medium. If there is a QGP, energy loss of heavy quarks yields an R_{AA} less than one.

2 Experimental setup

2.1 The ALICE detector

Part of the ongoing experiments at the LHC in CERN, the ALICE experiment is dedicated to the measurements of the properties of the strongly interacting matter such as the QGP. It's design allows it to measure the results of Pb-Pb colissions for center of mass energies up to 5.5 TeV. For these measurements, the detector consists of a central barrel assembly and a forward muon spectrometer. The latter is meant mainly for research into quarkonia, mesons which consist a quark and its corresponding anti-quark [8], and as such was not used in this research.

The central barrel assembly consists of a series of concentric, cylindrical detectors, all centered around the collision point. Of importance to this thesis are the Inner Tracking System (ITS) and the Time Projection Chamber (TPC). The central barrel as a whole has a pseudorapidity coverage of $|\eta| \leq 0.9$, corresponding to 45° away from the plane perpendicular to the beam axis (z).

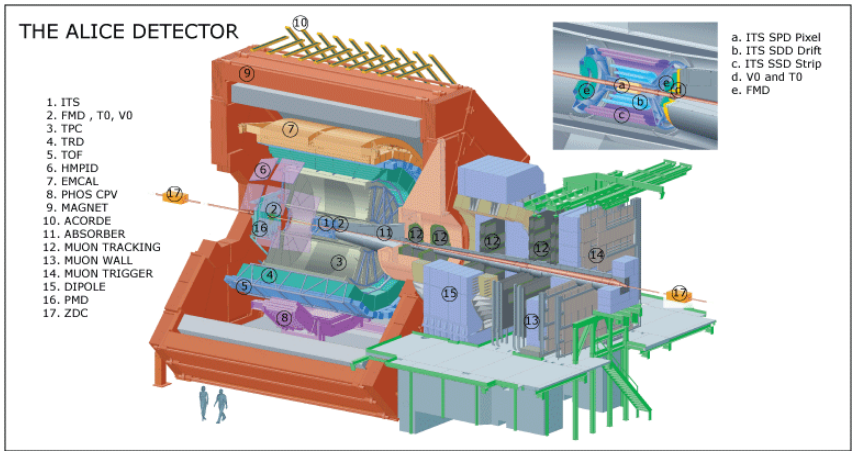

Figure 3: A schematic view of the ALICE detector, with its subdetectors labeled [9]. The central barrel is located within the solenoid magnet.

2.1.1 Inner Tracking System

The Inner Tracking System (ITS) is the detector closest to the beam axis and serves as the main vertexing detector of ALICE. In this capacity, the ITS serves to distinguish between particles produced in the collision of the heavy ions and particles produced by decay of short lived particles, such as the $B, D^{*+}$and D^0 mesons, which are of particular interest to this thesis. Additionally, it allows for the tracking of low momentum particles and increases the accuracy of the tracking performed in conjunction with the TPC.

The upgraded ITS consists of 7 layers of detector material, which are grouped into 3 radial groups as shown in Fig. 4. The group located closest to the collision point, consists of three layers of detector material, rather than the two layers in the current detector. These layers are also located closer to the interaction point, compared to the current ITS, which allows for more precise measurements of the impact parameter of passing particles. Perhaps the biggest change is that the all the detector material on the upgraded ITS will be digital pixel detectors, rather than the Silicon Drift and Silicon Strip detectors used in the outer barrel

of the current ITS detector. With this adoption of digital pixels for all detector layers, the ITS has no $\mathrm{d}E/\mathrm{d}x$ PID capability.

The upgraded ITS has a pseudo-rapidity acceptance from $|\eta| \leq 1.3$ in the outer layer, to $|\eta| \leq 2.5$ in the innermost layer.

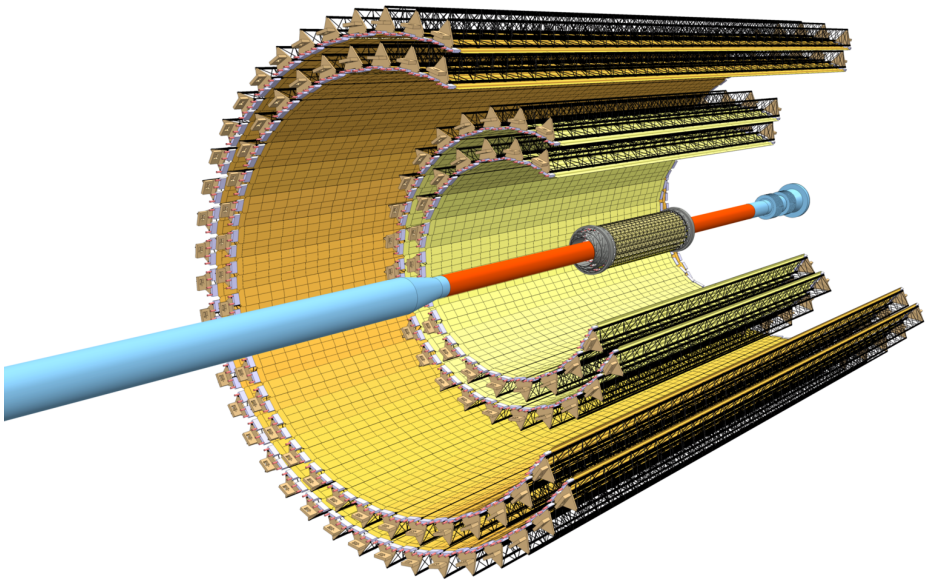

Figure 4: A schematic view of the upgraded ITS [10].

2.1.2 Time Projection Chamber

The Time Projection Chamber (TPC), shown in Fig. 5, is the main tracking detector of the ALICE experiment. It surrounds the ITS, making it the second closest detector to the interaction point. It is a cylindrical gas detector, filled with $88\mathrm{m}^3$ of $(90 : 10)$ $\mathrm{Ne}/\mathrm{CO}_2$ gas. The center plate of the detector serves as an electrode, inducing a uniform electric field along the beam-axis. As charged particles pass through the TPC, they ionize the gas. The freed electrons are then accelerated towards the readout chambers.

Besides serving as a means of tracking particles, the TPC can also be used to perform particle identification (PID) by measuring the energy lost ($\mathrm{d}E/\mathrm{d}x$) when traversing the detection gas.

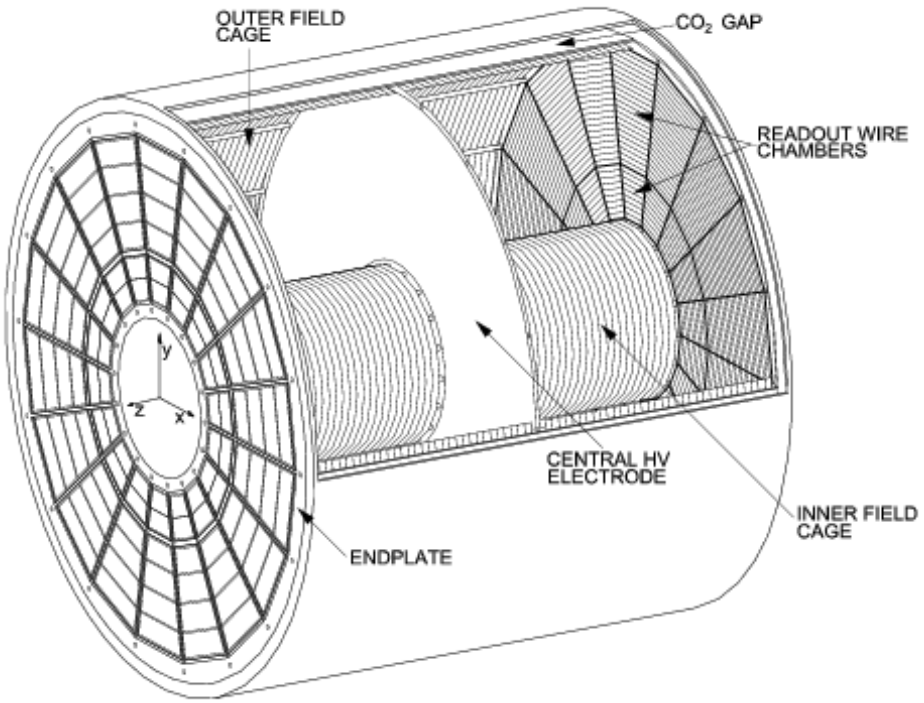

Figure 5: A schematic view of the TPC [11]

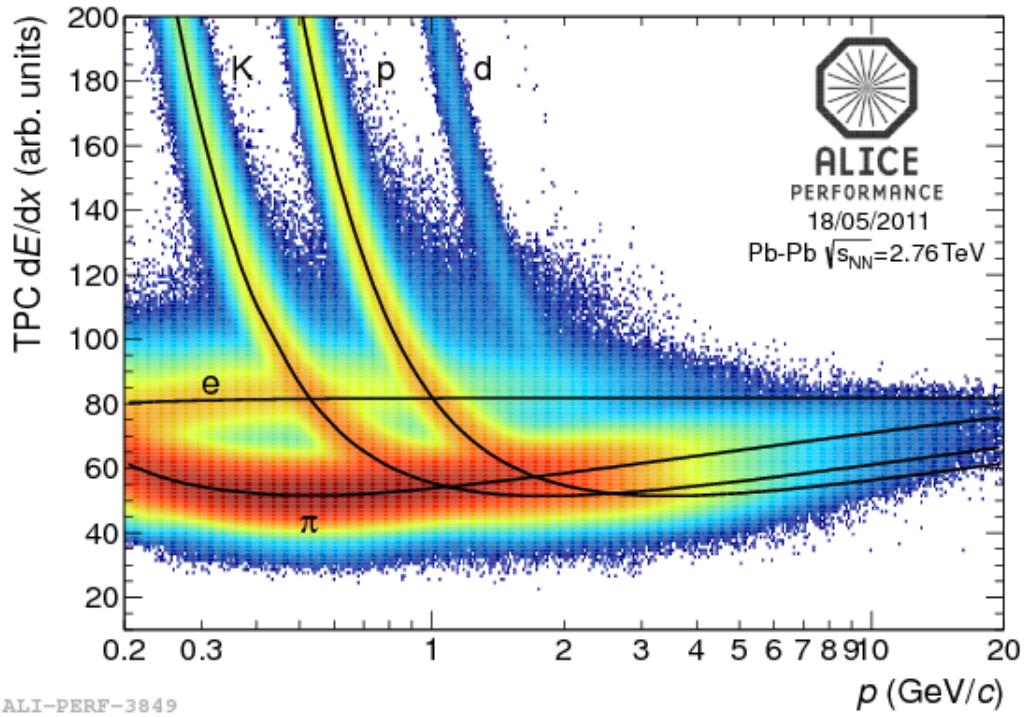

Figure 6: Measured energy loss versus momentum in TPC. The curves correspond with expected $\mathrm{d}E/\mathrm{d}x$ for the labeled particles [12].

2.2 Analysis Framework: (Ali)Root

Root is a object-oriented data analysis framework, originally developed by René Brun and Fons Rademakers [13]. It serves mainly as a tool for (particle) physicists to process large volumes of data. Despite coming with a set of visual tools, its main application in written C-style macros, which perform the required analysis. It comes equipped with a vast array of data display functionality, most notably in the form of histograms, as well as fitting functionalities which are of vital importance in this thesis in the determining the spread of the invariant mass of the D^{*+} signal.

AliRoot is an extension to the Root framework specifically designed for the ALICE project. It adds many ALICE specific code, such as particle tracks and Monte Carlo (MC) particles. The extension also allows the use of AliRoot as a simulator of collision events within the ALICE detector, via means of MC event generators and particle transportation simulators such as Pythia and Geant.

In this thesis, two datasets produced by Monte Carlo simulations were used:

MC10f7a is a charm forced simulation of p-p colissions at $\sqrt{s} = 13$ TeV in the current ALICE detector. One $c\bar{c}$ pair is produced per event in pseudorapidity $|\eta| < 1.2$. Produced D mesons decay hadronically in 80% of events and semileptonically in the remaining 20%.

MC_UPGRADE is a charm and beauty forced simulation of Pb-Pb collisions at $\sqrt{s_{NN}} =$ 5.5 TeV in the ALICE detector with the upgraded ITS. One B^0 meson decaying into $D^* + \pi^-$ is produced per event in pseudorapidity $|\eta| < 1$.

3 Improving the B^0 signal in Pb-Pb samples

A study was perfomed into the improvement of signal of the B^0 invariant mass by use of the upgraded ITS-detector. For this we use full Monte-Carlo simulations of Pb-Pb collisions in the upgraded ALICE detector. By accessing the Monte-Carlo data directly, we can find what combinations of reconstructed tracks constitute the actual signal of the B^0 and other mesons.

3.1 B^0 hadronic decay channel

In this thesis we on the reconstruction of the B^0 meson to a single decay channel. This channel consists of the following hadronic decays[1].

$$\begin{aligned} B^0 &\to D^{*+} + \pi^- \\ D^{*+} &\to D^0 + \pi^+ \\ D^0 &\to K^- + \pi^+ \\ \hline B^0 &\to K^- + 2\pi^+ + \pi^- \end{aligned}$$

Whilst this decay channel is fairly rare, with a branching ratio of only $(3.04\pm0.4)\cdot10^{-3}\%$ [14], this channel has the advantage that all of the final particles can be observed by the detector. Since the final products (a kaon and 3 pions) are all detectable, and by the conservation of momentum and energy, we can determine the invariant mass by

$$m_{inv} = \sqrt{(\sum_i E_i)^2 - (\sum_i \boldsymbol{p_i})^2}, \tag{4}$$

where E_i and $\boldsymbol{p_i}$ are the energies and momenta of the final product particles. However, reconstructing the invariant mass for 4 particles yields a combinatorial background which scales quartically with the number of particle tracks (if no PID is applied, as is the case in this thesis). In order to actually observe the B^0 meson, the signal (that is, the number of entries in the invariant mass spectrum due to particles that came from B^0), has to be discernible from the entries in the spectrum due to the combinatorial background. This discernibility has been quantised in the significance S_g

$$S_g = \frac{S}{\sqrt{S+B}}. \tag{5}$$

Here, S and B are the entries due to signal and combinatorial background (In a 3σ interval around the mean) respectively. In order to increase the significance, cuts must be applied to reduce the combinatorial background B, without completely decimating the signal S.

3.2 Cutting on D^* invariant mass

Since the relevant decay channel requires the presence of a D^{*+} meson, we wish cut away all the background triplets which do not amount to a D^{*+} mass. For this, it must first be

[1] The anti-particle version of this decay channel is also included in the statistical analysis

$D^{*+} p_T$ bin (GeV/c)	$\sigma_{current}$ (GeV/c^2)	$\sigma_{upgrade}$ (GeV/c^2)
1 - 3	0.012	0.010
3 - 5	0.016	0.012
5 - 8	0.019	0.017
8 - 16	0.024	0.016
16 - 24	0.046	0.019

Table 1: Invariant mass widths retrieved from fitted D^{*+} invariant mass signals in both current and upgraded ALICE detectors.

determined how accurately the new detector can detect the invariant mass of the signal of such true D^{*+} product triplets. By fitting the invariant mass spectrum with a Gaussian, we can determine a 3σ range around the D^* for which we can expect to cut with 99% signal retention.

For the determination of the width of the D^{*+} mass in the current ALICE detector, we used data from the MC10f7a Monte-Carlo simulation. The width for the upgrade is determined in a similar fashion via means of MC_UPGRADE simulation. The widths recovered from fitting the invariant mass signal with a Gaussian are shown in Fig. 7b and Table 1.

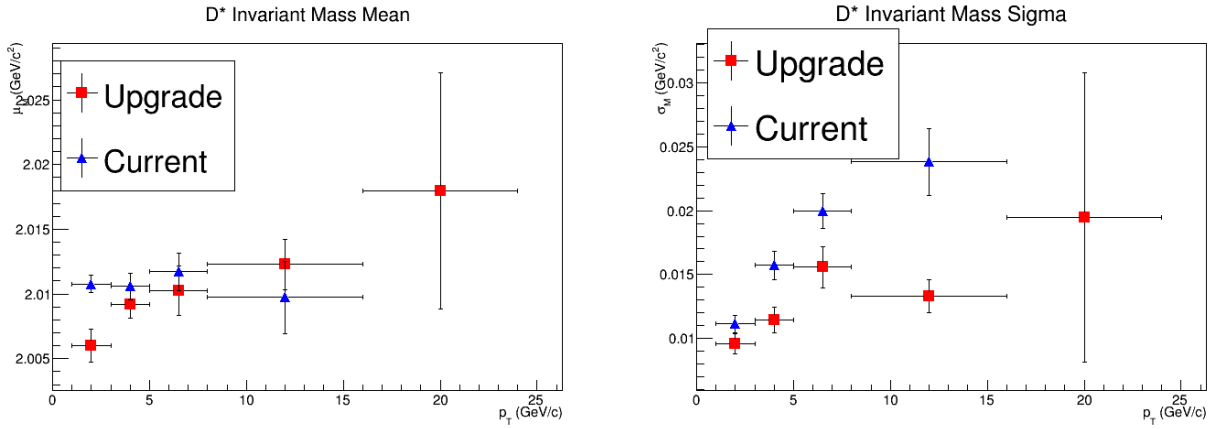

(a) (b)

Figure 7: Comparison of fitted D^{*+} invariant mass position (a) and width (b) for current and upgraded ALICE detector.

Applying cuts based on the fitted widths found above for the relevant D^{*+} p_T bins, and comparing these with the results with a standard cut we find that cutting on the D^{*+} invariant mass does allow for high signal retention.

$B^0 p_T$ (GeV/c)	S_{full}	$S_{current}$	$S_{upgrade}$
1 - 3	$(2.30 \pm 0.05) \times 10^{-2}$	$(2.17 \pm 0.05) \times 10^{-2}$	$(2.34 \pm 0.06) \times 10^{-2}$
3 - 5	$(3.15 \pm 0.06) \times 10^{-2}$	$(3.05 \pm 0.06) \times 10^{-2}$	$(3.27 \pm 0.07) \times 10^{-2}$
5 - 8	$(4.05 \pm 0.07) \times 10^{-2}$	$(3.94 \pm 0.06) \times 10^{-2}$	$(4.28 \pm 0.08) \times 10^{-2}$
8 - 16	$(4.87 \pm 0.07) \times 10^{-2}$	$(4.79 \pm 0.07) \times 10^{-2}$	$(5.17 \pm 0.08) \times 10^{-2}$
16 - 24	$(1.08 \pm 0.03) \times 10^{-2}$	$(1.04 \pm 0.03) \times 10^{-2}$	$(1.16 \pm 0.04) \times 10^{-2}$

Table 2: B^0 signals for cuts on the D^{*+} invariant mass.

As shown in table 4, we can see that the significance of the B^0 signal is higher for the upgraded cuts. This is with exception of the D^{*+} p_T interval [16, 24] GeV/c for which,

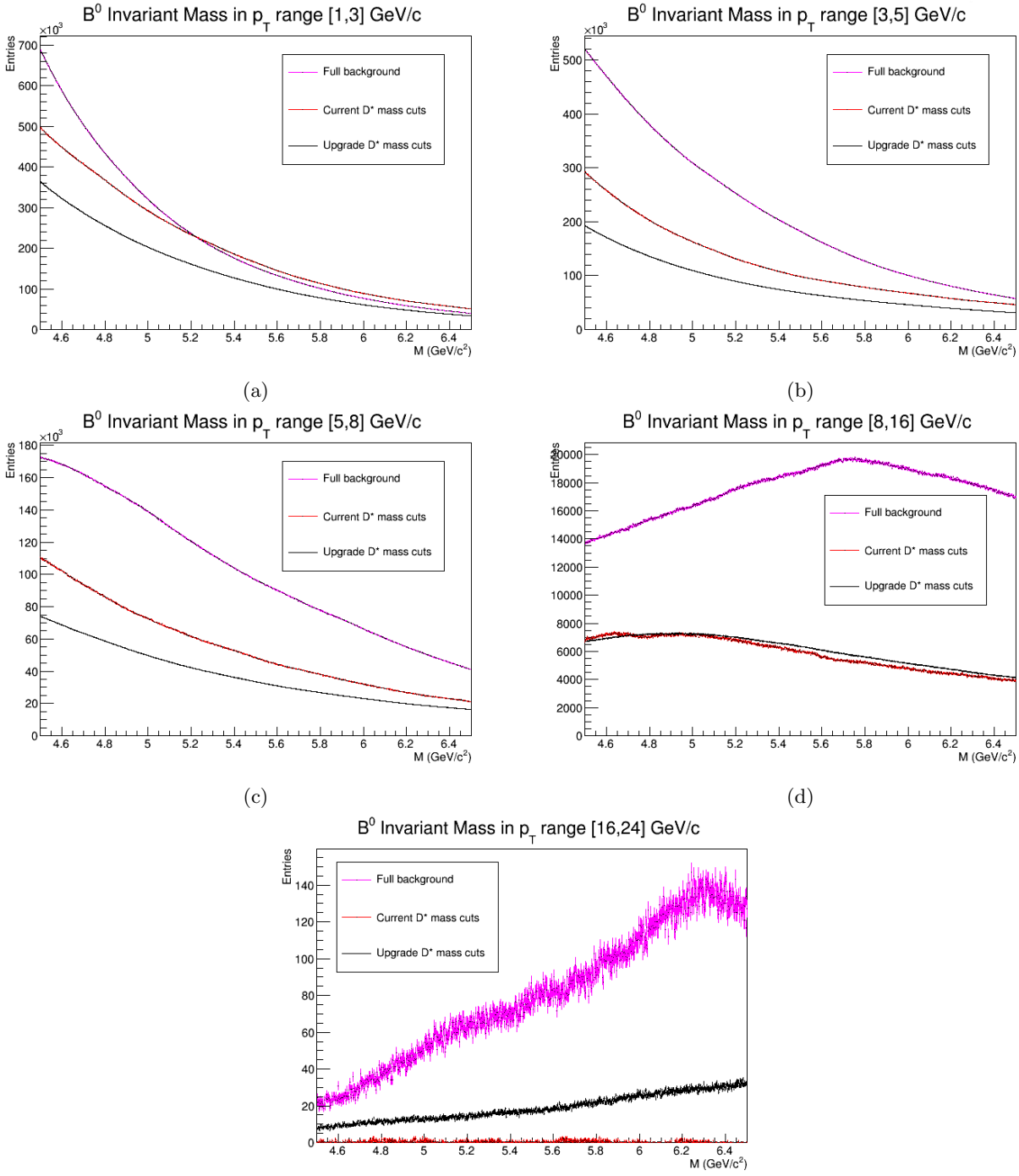

(a) (b) (c) (d) (e)

Figure 8: Comparison of background between D^{*+} invariant mass cuts: Standard background (cut on D^{*+} inv mass with $3\sigma = 0.074$ GeV/c^2), fitted sigma from current detector, fitted sigma from upgraded detector, for B^0 p_T intervals (a) 1-3, (b) 3-5, (c) 5-8, (d) 8-16 and (e) 16-24 GeV/c.

along with p_T interval [1,3] GeV/c, the background with the current cuts shows unphysical behaviour. In the first p_T interval the background is higher than the full background, of

B^0 p_T (GeV/c)	B_{full}	$B_{current}$	$B_{upgrade}$
1 - 3	$(1.914 \pm 1.7 \times 10^{-4}) \times 10^7$	$(1.946 \pm 2.5 \times 10^{-4}) \times 10^7$	$(1.334 \pm 6.9 \times 10^{-5}) \times 10^7$
3 - 5	$(2.129 \pm 1.9 \times 10^{-4}) \times 10^7$	$(1.114 \pm 1.9 \times 10^{-4}) \times 10^7$	$(7.612 \pm 5.2 \times 10^{-4}) \times 10^6$
5 - 8	$(1.153 \pm 1.4 \times 10^{-4}) \times 10^7$	$(5.876 \pm 1.4 \times 10^{-3}) \times 10^6$	$(4.028 \pm 3.8 \times 10^{-4}) \times 10^6$
8 - 16	$(2.220 \pm 6.1 \times 10^{-4}) \times 10^6$	$(8.168 \pm 5.2 \times 10^{-3}) \times 10^5$	$(8.478 \pm 1.7 \times 10^{-3}) \times 10^5$
16 - 24	$(9.978 \pm 4.1 \times 10^{-2}) \times 10^3$	73.67 ± 4.96	$(2.299 \pm 9.1 \times 10^{-3}) \times 10^3$

Table 3: B^0 background for cuts on the D^{*+} invariant mass.

B^0 p_T (GeV/c)	$S_{g,current}$	$S_{g,upgrade}$
1 - 3	4.92×10^{-6}	6.42×10^{-6}
3 - 5	9.14×10^{-6}	1.19×10^{-5}
5 - 8	1.63×10^{-5}	2.14×10^{-5}
8 - 16	5.30×10^{-5}	5.62×10^{-5}
16 - 24	1.22×10^{-3}	2.43×10^{-4}

Table 4: Signficance of the B^0 invariant mass signal for current and upgraded D^{*+} invariant mass cuts.

which it is a subset. In the last p_T interval, the background with the current cuts is lower than the background with the (stricter) upgraded cuts. Since whatever passes the upgraded cuts automatically also satisfies the current cuts, the background of the upgraded cuts should be included in the current background. It is likely that this is due to the low number of events processed with the current cuts.

3.3 Additional cuts

Whilst tables 2 and 3 show that the application of a cut on the D^{*+} invariant mass cuts away background without affecting the signal, this cut alone is not enough to improve the statistical significance noticably. For this, we require additional cuts. In the following section, we investigate the effectiveness of applying several additional cuts.

3.3.1 $D^{*+} - D^0$ invariant mass difference cut

Since the difference in invariant mass (ΔM) between the D^{*+} and the D^0 mesons is a physical value, 99% of actual D^{*+} mesons have to lie within a 3σ range around this value. This allows for a second cut on the D^{*+} candidates, obtained after the aforementioned upgraded invariant mass cut. Again, this cut should result in only 1% signal loss. For the determination of the σ in the ΔM, we fitted the ΔM signal, produced in the Monte Carlo simulations of the fully upgraded detector, see table 5.

Application of these additional cuts yields the signals and background as shown in table 5 and Fig. 9. Whilst little signal is lost in this cut, the random $(K\pi\pi\pi)$-couples which form the combinatorial background still dominate, causing the statistical significance to be very small.

$\boldsymbol{D^{*+}p_T}$ **bin (GeV/c)**	$\boldsymbol{\sigma_{\Delta M}}$ **(GeV/c^2)**
1 - 3	6.0×10^{-4}
3 - 5	5.0×10^{-4}
5 - 8	4.6×10^{-4}
8 - 16	2.8×10^{-4}
16 - 24	5.2×10^{-4}

Table 5: Delta mass widths retrieved from fitted ΔM invariant mass signals in upgraded ALICE detector.

$\boldsymbol{B^0 p_T}$ **(GeV/c)**	$\boldsymbol{S_{\Delta M}}$	$\boldsymbol{B_{\Delta M}}$
1 - 3	$(2.15 \pm 0.04) \times 10^{-2}$	1.58×10^4
3 - 5	$(2.99 \pm 0.06) \times 10^{-2}$	1.86×10^4
5 - 8	$(3.91 \pm 0.06) \times 10^{-2}$	9.59×10^4
8 - 16	$(4.72 \pm 0.07) \times 10^{-2}$	2.14×10^4
16 - 24	$(1.03 \pm 0.04) \times 10^{-2}$	2.37×10^2

Table 6: Signal and background for the B^0 invariant mass with additional ΔM cuts applied on top of D^{*+} invariant mass cuts in the upgraded ALICE detector.

$\boldsymbol{B^0}$ $\boldsymbol{p_T}$ **(GeV/c)**	$\boldsymbol{S_{g,\Delta M}}$
1 -3	1.71×10^{-4}
3 -5	$6,94 \times 10^{-5}$
5 - 8	1.26×10^{-4}
8 - 16	3.23×10^{-4}
16 - 24	6.68×10^{-4}

Table 7: Significance of the B^0 signal with additional cuts on ΔM are applied.

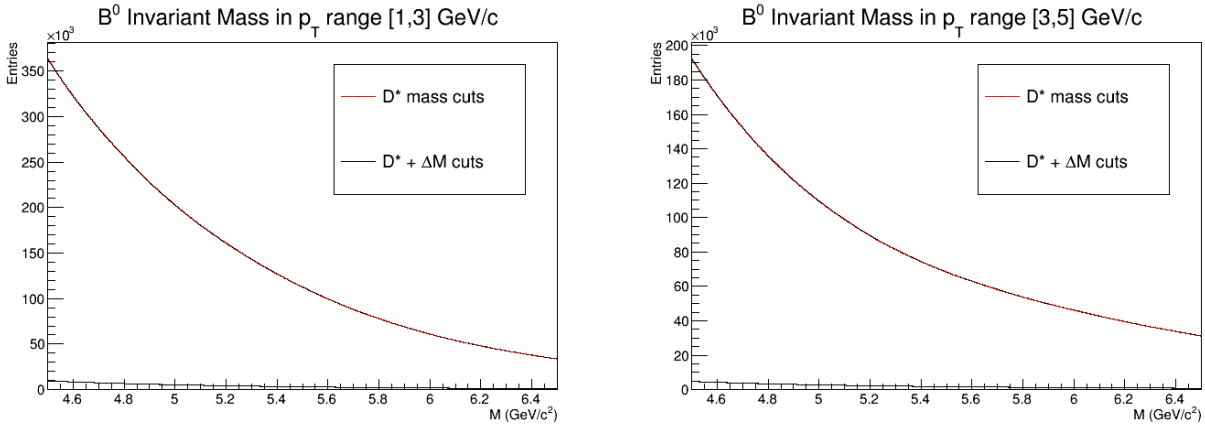

(a)

(b)

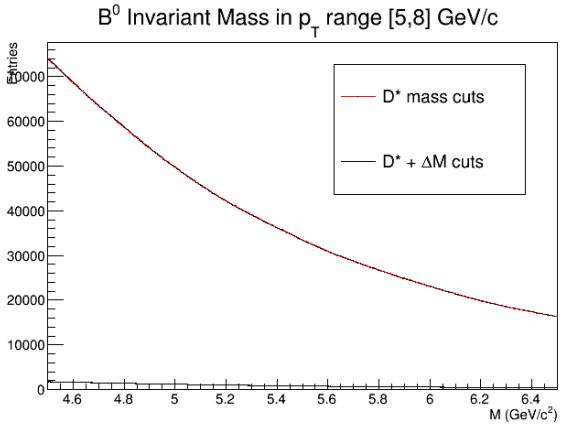

(c)

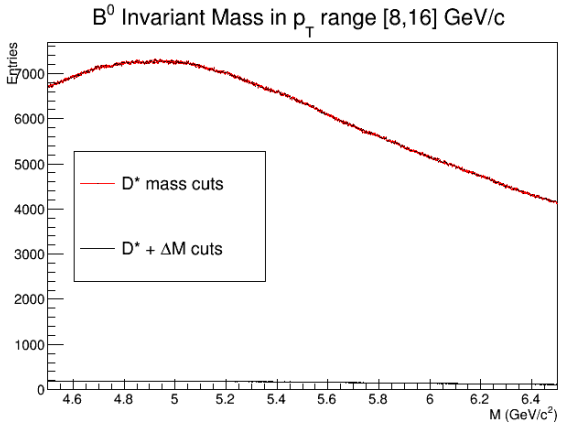

(d)

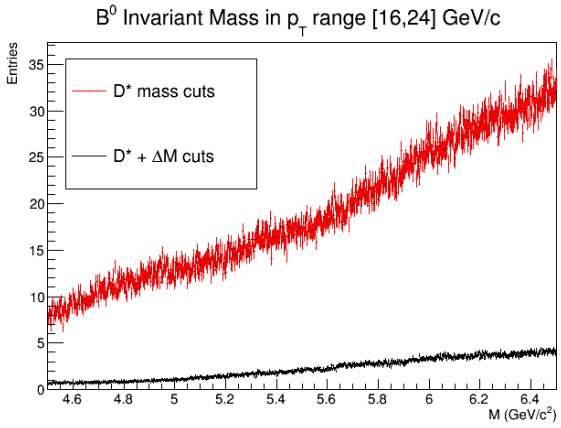

(e)

Figure 9: Comparison of background between the upgraded D^{*+} invariant mass cut and the upgraded D^{*+} invariant mass cuts with an additional cut on the ΔM invariant mass difference, for B^0 p_T intervals (a) 1-3, (b) 3-5, (c) 5-8, (d) 8-16 and (e) 16-24 GeV/c.

3.3.2 Kaon: impact parameter study

Another class of cuts we can apply is on the Distance of Closest Approach (DCA) or impact parameter of particles. Since the kaon is one of the last particles to be produced in the decay channel, we expect those kaons to have a larger DCA than prompt kaons. Cutting on the DCA tends to remove a lot of signal as well, as shown in Fig. 10. We therefore looked at a set of different DCA cuts (table 8), in order to see which cut offers the best background reduction vs signal retention.

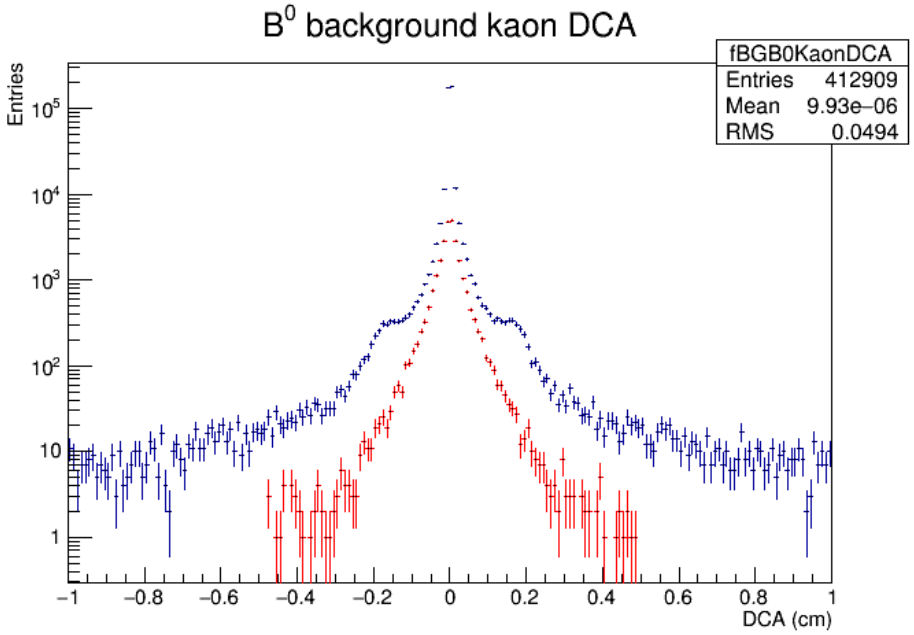

Figure 10: DCA of kaons from signal (B^0, red symbols) and background plus signal (blue symbols).

$B^0 p_T$ (GeV/c)	S(DCA $\leq 50\mu$m)	S(DCA $\leq 100\mu$m)
1 - 3	$(1.37 \pm 0.13) \times 10^{-3}$	$(3.64 \pm 0.67) \times 10^{-4}$
3 - 5	$(3.47 \pm 0.20) \times 10^{-3}$	$(7.77 \pm 0.97) \times 10^{-4}$
5 - 8	$(6.67 \pm 0.28) \times 10^{-3}$	$(2.16 \pm 0.16) \times 10^{-3}$
8 - 16	$(9.41 \pm 0.33) \times 10^{-3}$	$(3.35 \pm 0.20) \times 10^{-3}$
16 - 24	$(1.77 \pm 0.14) \times 10^{-3}$	$(6.92 \pm 0.92) \times 10^{-4}$
	S(DCA $\leq 150\mu$m)	S(DCA $\leq 200\mu$m)
1 - 3	$(1.56 \pm 0.67) \times 10^{-4}$	$(6.06 \pm 3.03) \times 10^{-5}$
3 - 5	$(2.59 \pm 0.58) \times 10^{-4}$	$(1.06 \pm 0.40) \times 10^{-4}$
5 - 8	$(8.17 \pm 1.02) \times 10^{-4}$	$(2.73 \pm 0.64) \times 10^{-4}$
8 - 16	$(1.41 \pm 0.14) \times 10^{-3}$	$(5.90 \pm 0.95) \times 10^{-4}$
16 - 24	$(3.76 \pm 0.70) \times 10^{-4}$	$(2.12 \pm 0.57) \times 10^{-4}$

Table 8: Signal for the B^0 invariant mass for various DCA cuts applied on top of ΔM cuts and D^{*+} invariant mass cuts in the upgraded ALICE detector.

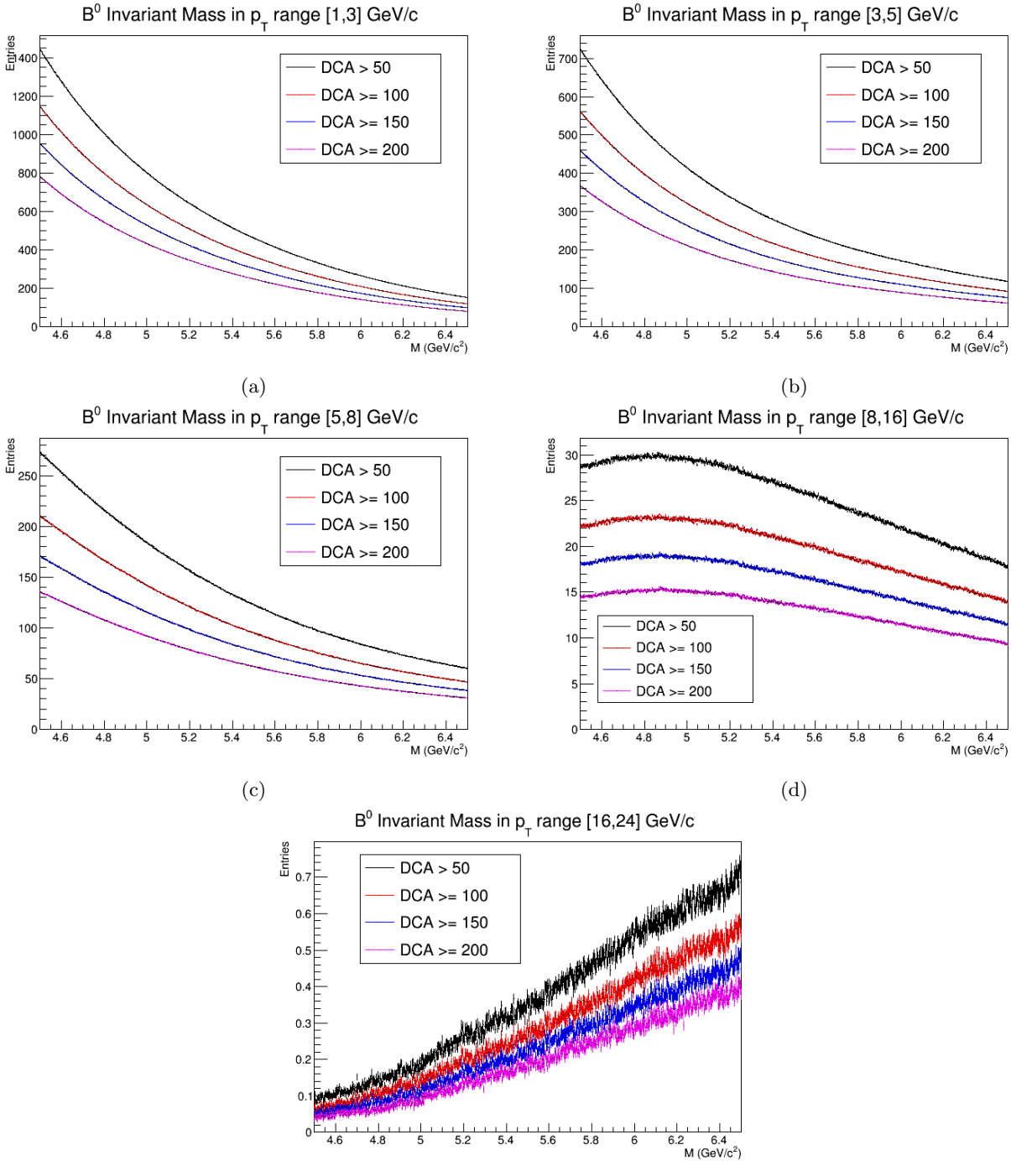

Figure 11: Comparison of background between multiple kaon DCA cuts, for B^0 p_T intervals (a) 1-3, (b) 3-5, (c) 5-8, (d) 8-16 and (e) 16-24 GeV/c.

From table 9 we can conclude that the cut DCA $< 50\mu$m ensures the best significance for the data. However, when compared to the significance obtained by merely applying a D^{*+} invariant mass and ΔM mass difference cut as shown in table 7, we find that applying any of the above DCA cuts results in a reduction of the significance. The DCA cut therefore is not a viable cut in order to improve signal significance.

B^0 p_T (GeV/c)	S_g(DCA $< 50\mu$m)	S_g(DCA $< 100\mu$m)	S_g(DCA $< 150\mu$m)	S_g(DCA $< 200\mu$m)
1 - 3	4.59×10^{-6}	1.37×10^{-6}	6.43×10^{-7}	2.77×10^{-7}
3 - 5	1.59×10^{-5}	4.05×10^{-6}	1.49×10^{-6}	6.79×10^{-7}
5 - 8	4.46×10^{-5}	1.64×10^{-5}	6.89×10^{-6}	2.57×10^{-6}
8 - 16	1.45×10^{-4}	5.84×10^{-5}	2.72×10^{-5}	1.27×10^{-5}
16 - 24	2.72×10^{-4}	1.22×10^{-4}	7.32×10^{-5}	4.57×10^{-5}

Table 9: Significance of the B^0 invariant mass signal for various DCA cuts.

3.3.3 Soft pion: transverse momentum study

A final cut we implemented was on the transverse momentum of the soft pion. Since these pions are formed when an excited D^{*+} decays into the D^0, they carry less energy. For this reason, we implemented a cut on the maximum p_T for the soft pions. In addition to reducing the combinatorics, it has the added advantage of allowing early rejection of $(K\pi\pi)$-triples, which speeds up computation of the combinatorial background.

However, as shown in Figs. 12 - 15, we can see that the effect on the background is negligible. The background after the cut is also higher than without the cut, this is probably due to a difference in statistics. As such, the soft pion transverse momentum cut is not viable as a means to reduce background, which can be attributed to the fact that most of the background which would have been cut has already been excluded by the cuts on the D^{*+} mass.

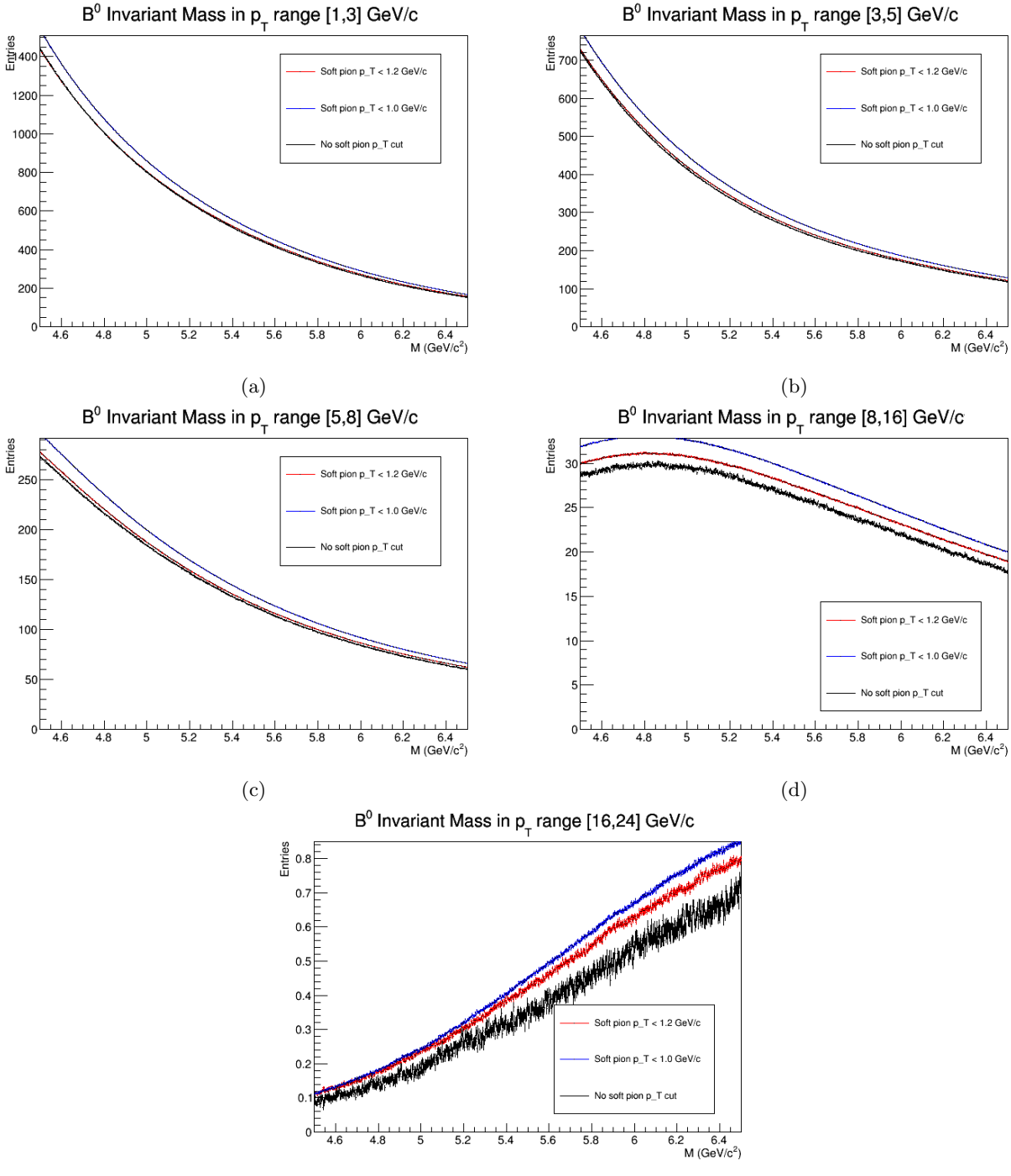

Figure 12: Comparison of background between soft pion p_T cuts on top of DCA cut < 50 μm, for B^0 p_T intervals (a) 1-3, (b) 3-5, (c) 5-8, (d) 8-16 and (e) 16-24 GeV/c.

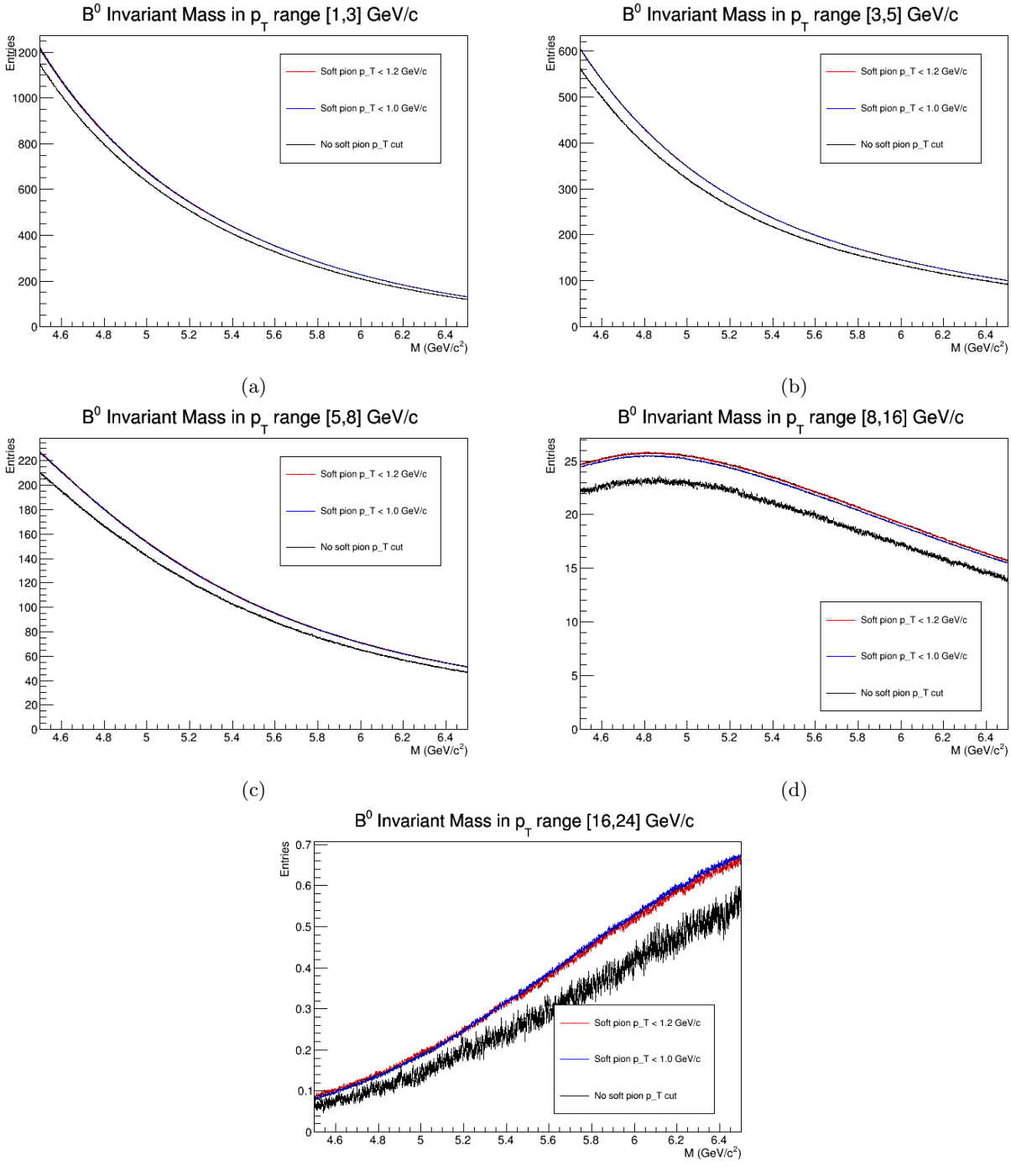

Figure 13: Comparison of background between soft pion p_T cuts on top of DCA cut < 100 μm, for B^0 p_T intervals (a) 1-3, (b) 3-5, (c) 5-8, (d) 8-16 and (e) 16-24 GeV/c.

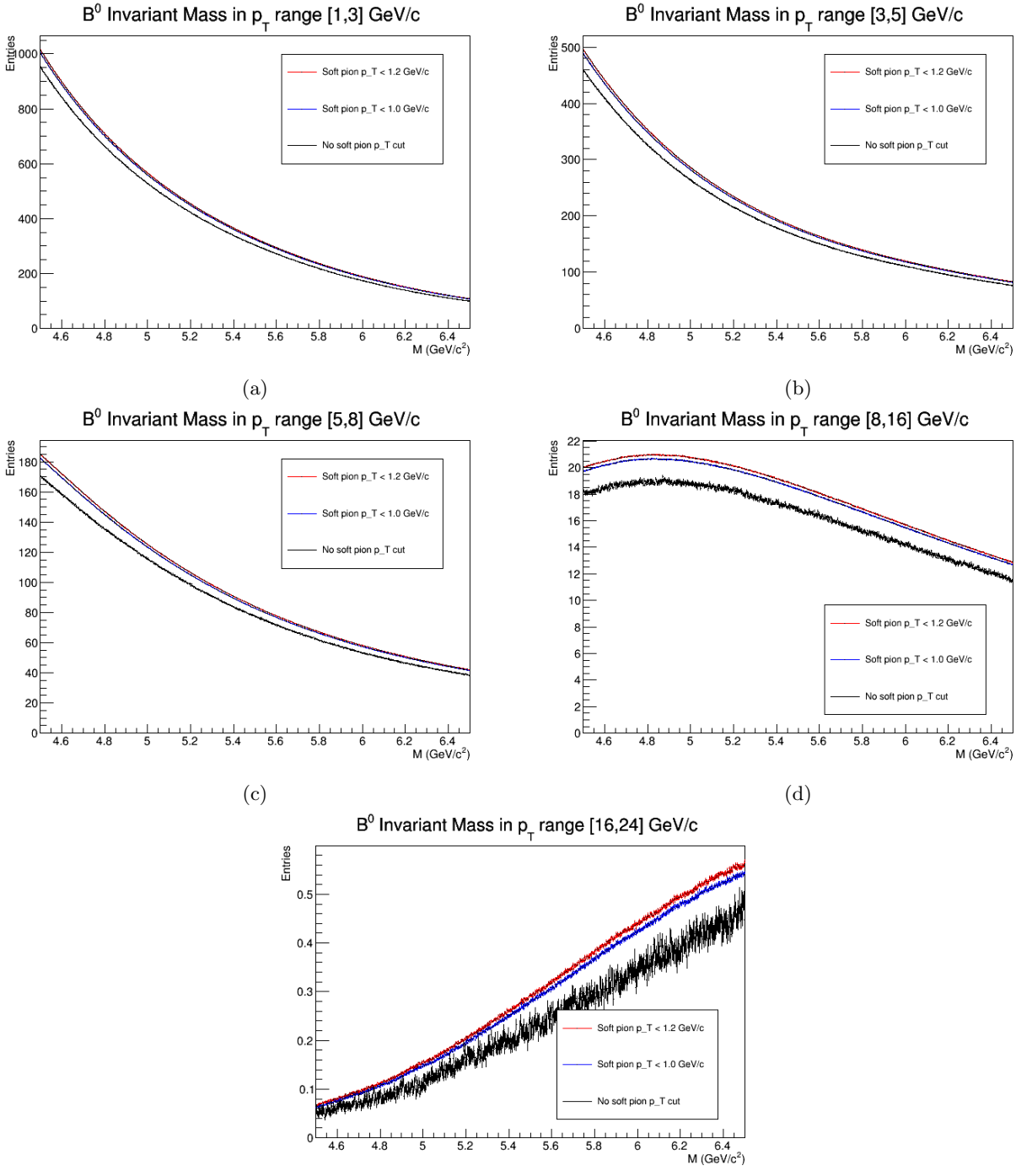

Figure 14: Comparison of background between soft pion p_T cuts on top of DCA cut < 150 μm, for B^0 p_T intervals (a) 1-3, (b) 3-5, (c) 5-8, (d) 8-16 and (e) 16-24 GeV/c.

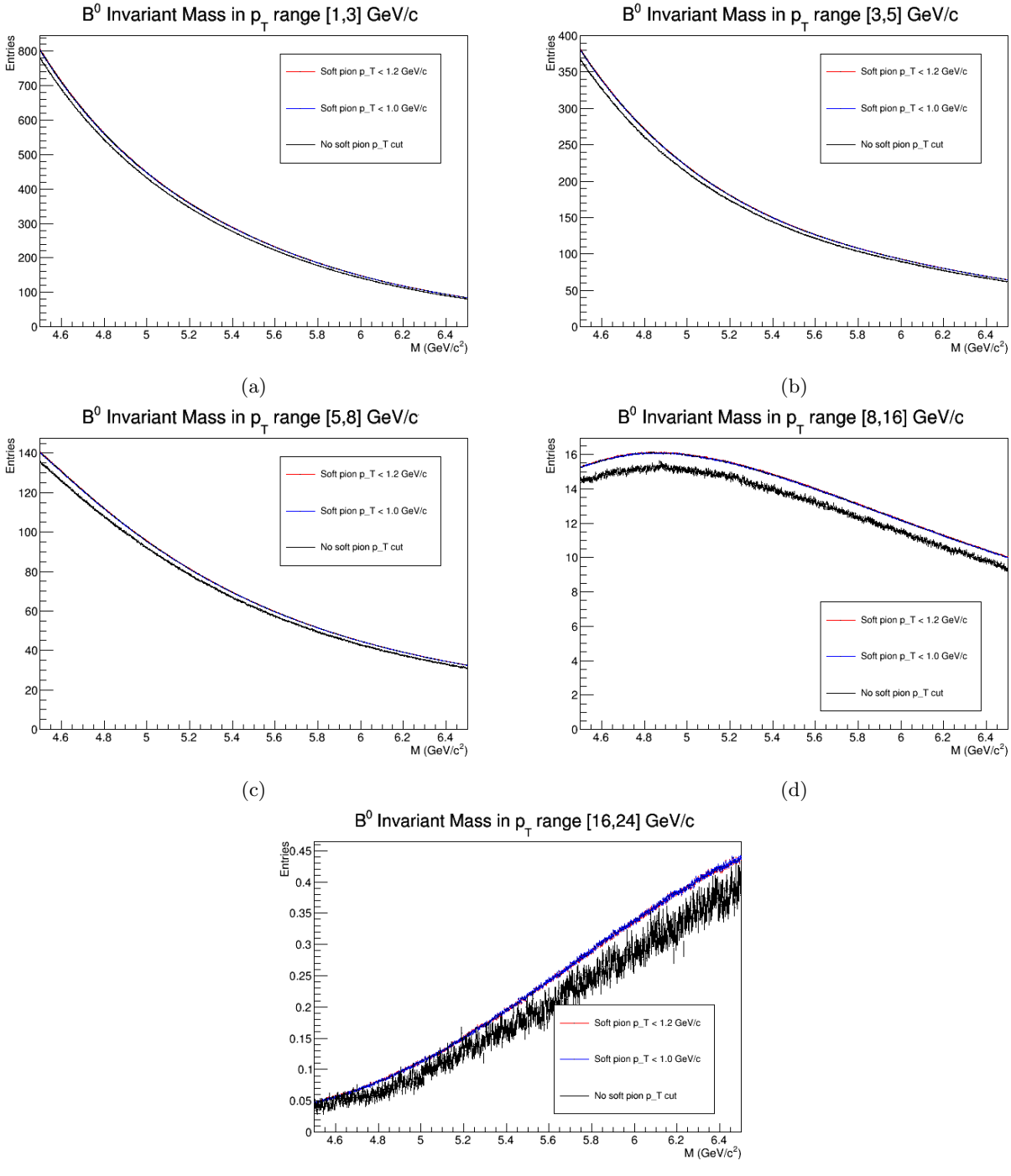

Figure 15: Comparison of background between soft pion p_T cuts on top of DCA cut < 200 μm, for B^0 p_T intervals (a) 1-3, (b) 3-5, (c) 5-8, (d) 8-16 and (e) 16-24 GeV/c.

4 Discussion and Outlook

We have found that the upgraded ITS allows the determining of the D^{*+} invariant mass with a smaller width. This, in turn, allows the application of stricter cuts on the invariant mass the D^{*+}. We have shown that this improvement in accuracy leads to a reduction in background contribution and an increase in B^0 signal significance. Though some issues remain with physically impossible background distributions of the B^0 invariant mass with cuts based on current detector performance. Additional analysis of events using these cuts is required in order to determine the cause of these issues.

We also investigated the effects of additional cuts. In this we have found that the application of a cut on the mass difference ΔM can improve the significance by an order of magnitude. Furthermore we investigated the feasibility of cuts on the kaon DCA and soft pion transverse momentum. Unfortunately, neither was found to be suitable for use in cutting the background. The former is unsuitable due to the detrimental effect on signal and thereby the significance, the latter has shown no positive effect on reducing the combinatorial background.

As the significance still is far below observation levels, additional studies into cutting parameters is required. Other potential improvements due to the upgraded ITS were also not taken into consideration. One such area which could show improvement is the kaon DCA, as this depends highly on the spatial resolution of the (upgraded) ITS. Other studies can include cuts on primary vertexes of particles.

References

[1] B. Heinemann, "Future of LHC", http://www.sns.ias.edu/ckfinder/userfiles/files/Heinemann-PiTP-II.pdf, July 2013.

[2] G. Aad *et al.* (ATLAS Collaboration), "Observation of a new particle in the search for the Standard Model Higgs boson with the ATLAS detector at the LHC", Phys. Lett. B **716** (2012) 1-29, [arXiv:1207.7214].

[3] MissMJ, "Standard Model of Elementary Particles", http://upload.wikimedia.org/wikipedia/commons/0/00/Standard_Model_of_Elementary_Particles.svg, 2014.

[4] F. Muheim, "Quantum Chromodynamics (QCD)" (lecture notes), http://www2.ph.ed.ac.uk/ muheim/teaching/partphys/qcd.ps, University of Edinburgh, 2004.

[5] Brookhaven National Laboratory, "Closing in on the Border Between Primordial Plasma and Ordinary Matter", http://www.bnl.gov/rhic/news2/news.asp?a=1446&t=pr, April 2015.

[6] F. M. Liu and S. X. Liu, "Quark-gluon plasma formation time and direct photons from heavy ion collisions," Phys. Rev. C **89** (2014) 3, 034906 [arXiv:1212.6587 [nucl-th]].

[7] M. Djordjevic and M. Gyulassy, "Where is the charm quark energy loss at RHIC?," Phys. Lett. B **560** (2003) 37 [nucl-th/0302069].

[8] The ALICE Collaboration, "The ALICE Dimuon Spectrometer", http://aliceinfo.cern.ch/Public/en/Chapter2/Chap2_dim_spec.html, June 2015.

[9] The ALICE Collaboration, "The ALICE Experiment", http://aliceinfo.cern.ch/Public/en/Chapter2/Chap2Experiment-en.html, June 2015.

[10] B. Abelev *et al.* [ALICE Collaboration], "Technical Design Report for the Upgrade of the ALICE Inner Tracking System," J. Phys. G **41** (2014) 087002.

[11] C. Lippmann, "Particle identification," Nucl. Instrum. Meth. A **666** (2012) 148 [arXiv:1101.3276 [hep-ex]].

[12] P. Christiansen [ALICE Collaboration], "High p_t identified particle production in ALICE," Nucl. Phys. A **910-911** (2013) 20 [arXiv:1208.5368 [nucl-ex]].

[13] R. Brun and F. Rademakers, "ROOT An object oriented data analysis framework", Nucl. Instrum. Meth. A **398** (1997) 81 - 86.

[14] L. Vermunt, "Performance studies for the measurement of B^0 mesons in proton-proton collisions at 13 TeV with the ALICE experiment", Bachelor thesis, Utrecht University, 2015.